Supporting Information

PEI-Based Nanocomposite with Dual-Functionally Complementary Fillers for Synergistic Enhancement of Energy Storage Performance

Qiaoyu Yang [a], *Ying Lin*[*a], *Yanlong Ma* [a], *Zhener Dang* [a], *Min Yang* [a], *Gaoyuan Xuan* [b], *Qibin Yuan*[*b] and *Haibo Yang*[*a]

a.School of Materials Science and Engineering, Shaanxi Key Laboratory of Green Preparation and Functionalization for Inorganic Materials, Shaanxi University of Science and Technology, Xi'an 710021, China

b. School of Electronic Information and Artificial Intelligence, Shaanxi University of Science and Technology, Xi'an, Shaanxi 710021, China.

*Corresponding authors:

(Ying Lin[*a]) E-mail: linying@sust.edu.cn

(Qibin Yuan[*b]) E-mail: yuanqibin-sust@163.com

(Haibo Yang[*a]) E-mail: yanghaibo@sust.edu.cn

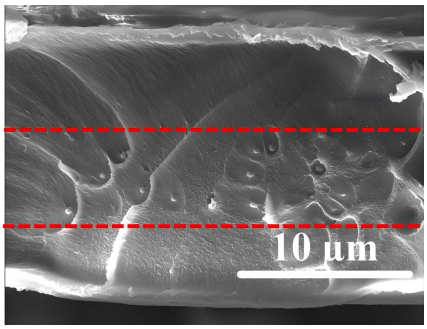

Fig. S1. Cross-sectional SEM image of P-0.5Z-P .

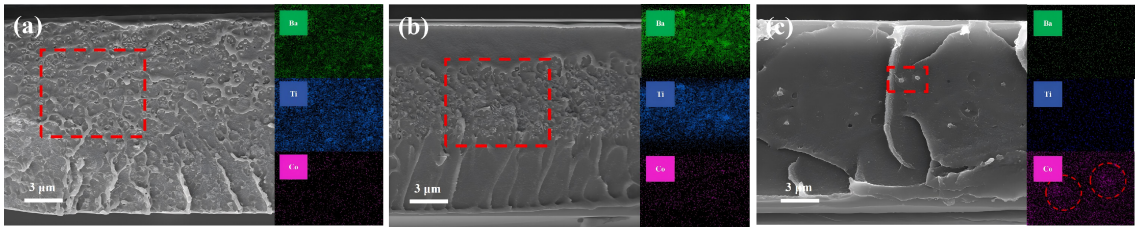

Fig. S2 Cross-sectional EDX mapping of (a) P/0.5ZB, (b) P-0.5ZB-P, and (c) P-0.5Z-P.

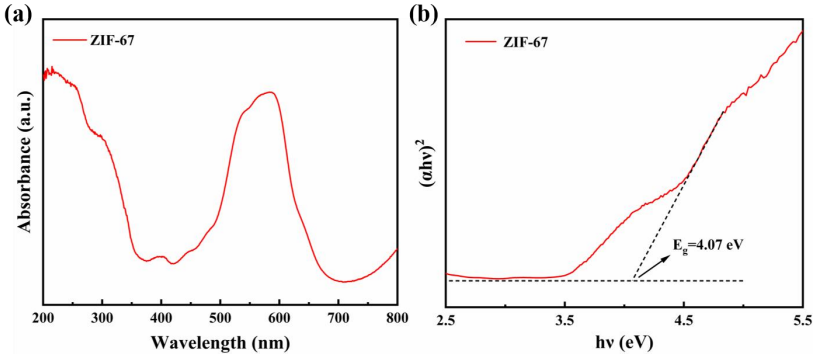

Fig. S3. (a) UV-Vis absorption spectrum and (b) $(\alpha h\nu)^2$-hν plot of ZIF-67.

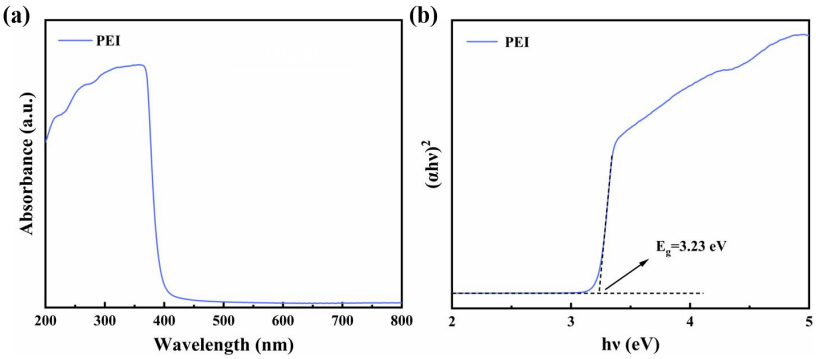

Fig. S4. (a) UV-Vis absorption spectrum and (b) $(\alpha h\nu)^2$-hν plot of PEI.

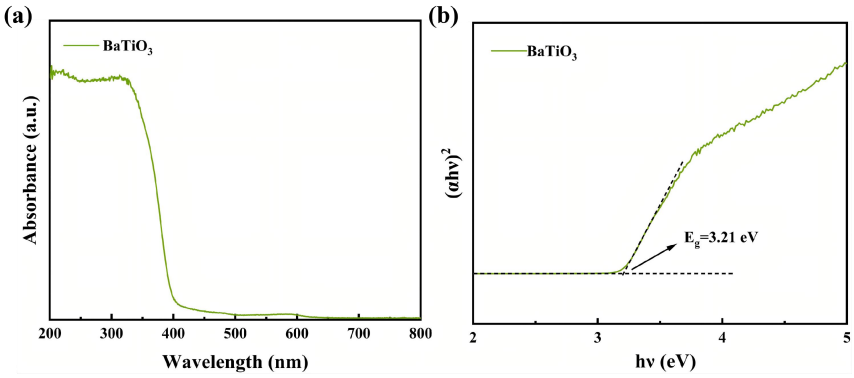

Fig. S5. (a) UV-Vis absorption spectrum and (b) $(\alpha h\nu)^2$-hν plot of $BaTiO_3$ NPs.

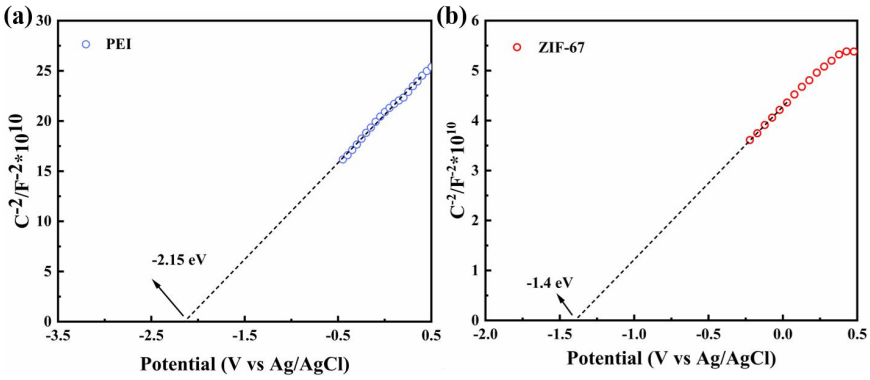

Fig. S6. Mott-Schottky plot of (a) ZIF-67and (b) PEI.

Fig. S3 to 5 displays the UV-Vis absorption spectra and the $(\alpha h\nu)^2$-hν plots of ZIF-67 and PEI. Fig. S6 displays the Mott-Schottky curves of ZIF-67 and PEI. The results show that the band gaps of ZIF-67, PEI, and $BaTiO_3$ NPs are 4.07 eV, 3.23 eV, and 3.21 eV respectively, indicating a discrepancy in their band structures[1,2].

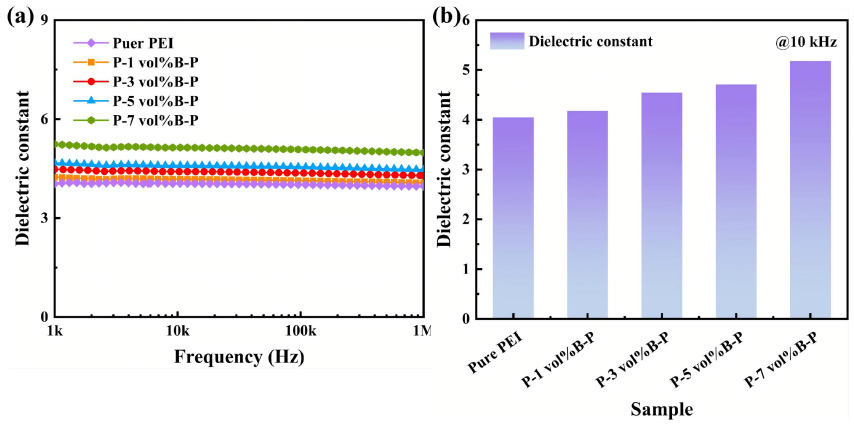

Fig. S7. (a) Frequency dependence of ε_r and (b) precise ε_r values at 10 kHz for P-B-P with different $BaTiO_3$ NPs contents.

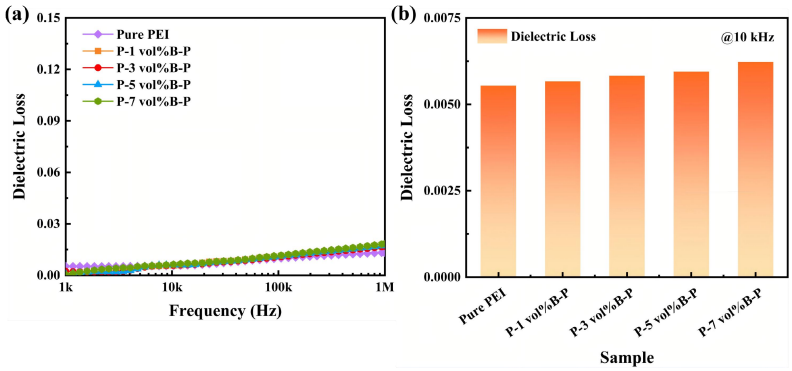

Fig. S8. (a) Frequency dependence of tanδ and (b) precise tanδ values at 10 kHz for P-B-P with different $BaTiO_3$ NPs contents.

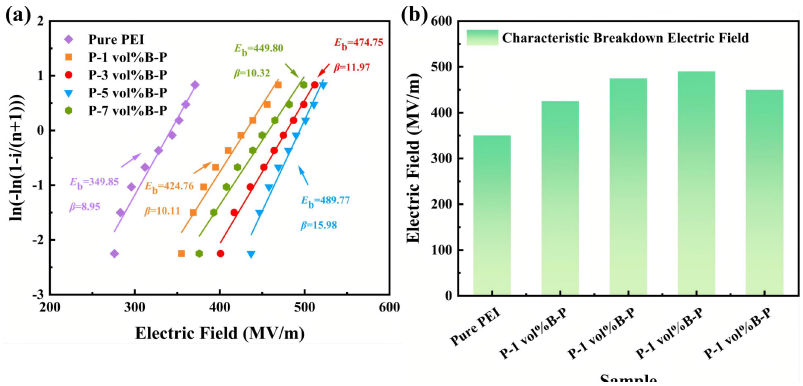

Fig. S9. (a) Weibull distribution and (b) characteristic breakdown strength of P-B-P with different $BaTiO_3$ NPs contents.

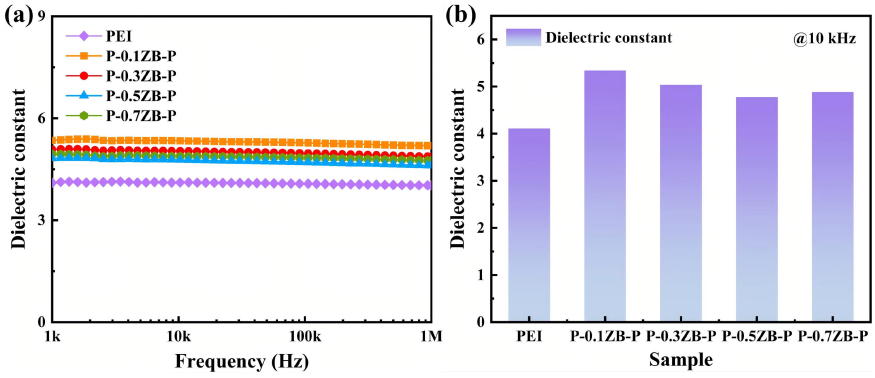

Fig. S10. Frequency dependence of (a) ε_r and (b) precise ε_r values at 10 kHz for P-ZB-P with different ZIF-67 contents.

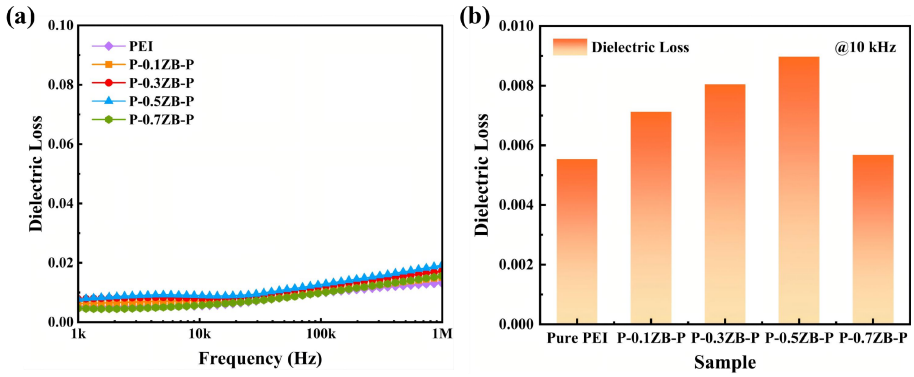

Fig. S11. Frequency dependence of (a) tanδ and (b) precise tanδ values at 10 kHz for P-ZB-P with different ZIF-67 contents.

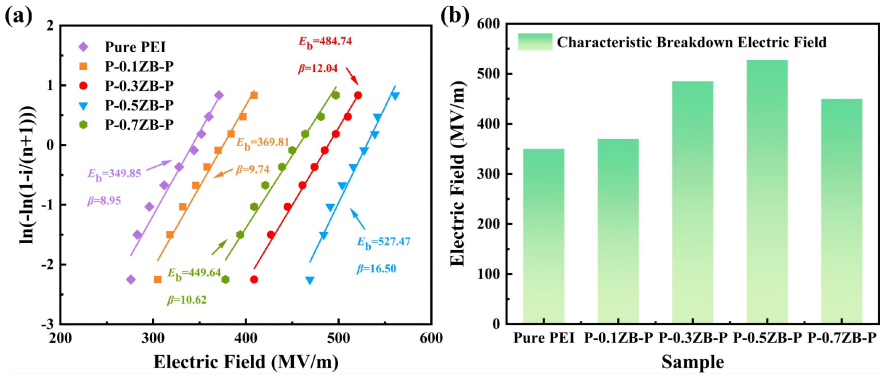

Fig. S12. (a) Weibull distribution and (b) characteristic breakdown strength of P-ZB-P with different ZIF-67 contents.

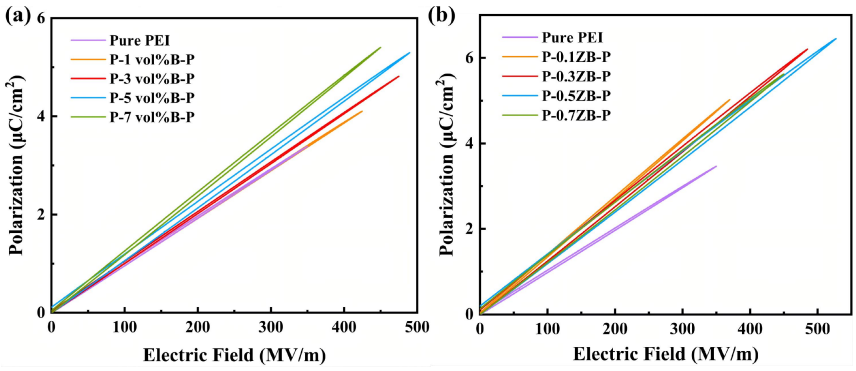

Fig. S13. (a) *P-E* loops of P-B-P with different $BaTiO_3$ NP contents and (b) P-ZB-P with different ZIF-67 contents.

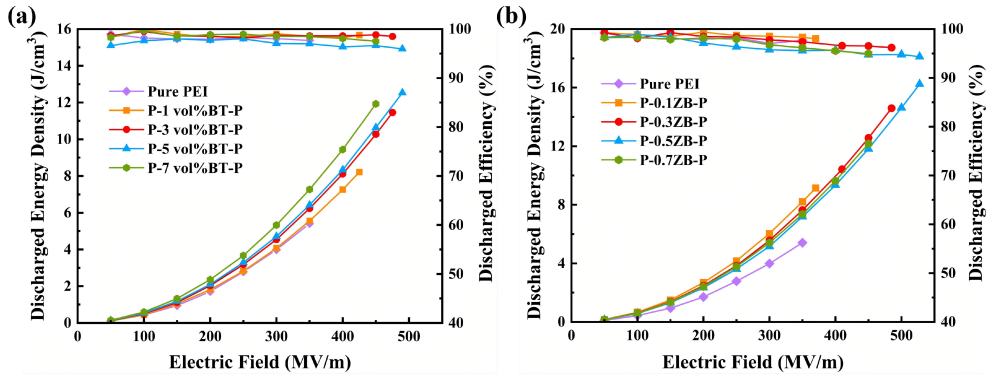

Fig. S14. U_e and η of (a) P-B-P with different $BaTiO_3$ NP contents and (b) P-ZB-P with different ZIF-67 contents.

In this experiment, a series of films including P-B-P and P-ZB-P were fabricated. Fig. S7 to 9, Fig. S12 and 13 present the dielectric and energy storage properties of the P-B-P nanocomposites. Among them, the sample with a middle layer containing 24.64 wt% $BaTiO_3$ NPs, denoted as P-24.64B-P (where "B" in the text represents 24.64B), exhibited the optimal performance. Based on this, ZIF-67 was incorporated into the middle blend layer to prepare P-ZB-P nanocomposites, with the best-performing sample being P-0.5ZB-P (as shown in Fig. S10 to 14). Finally, P/0.5ZB, P-0.5ZB-P, and P-0.5Z-P were prepared as control groups, and their dielectric properties and energy storage performance were characterized.

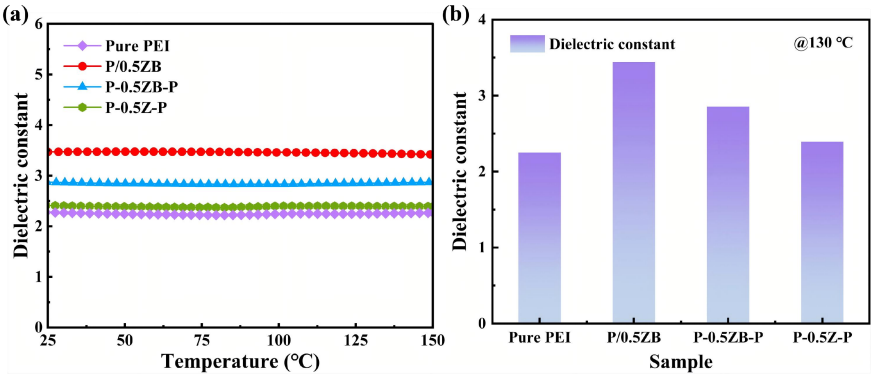

Fig. S15. Temperature dependence of (a) ε_r and (b) precise ε_r values at 130 °C for pure PEI, P/0.5ZB, P-0.5ZB-P, and P-0.5Z-P.

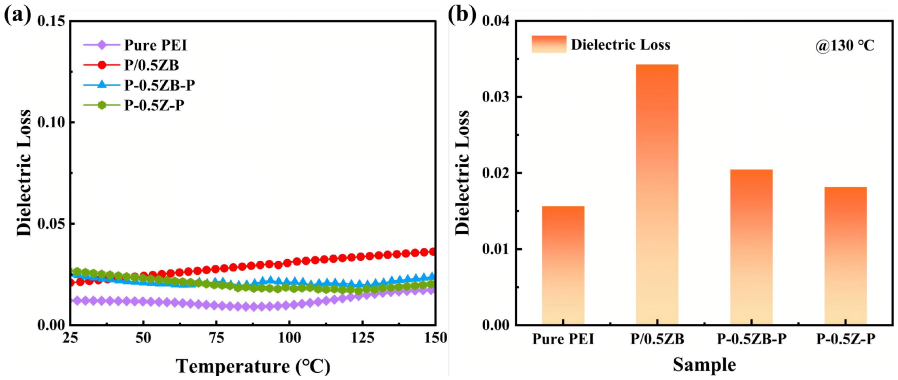

Fig. S16. Temperature dependence of (a) tanδ and (b) precise tanδ values at 130 °C for pure PEI, P/0.5ZB, P-0.5ZB-P, and P-0.5Z-P.

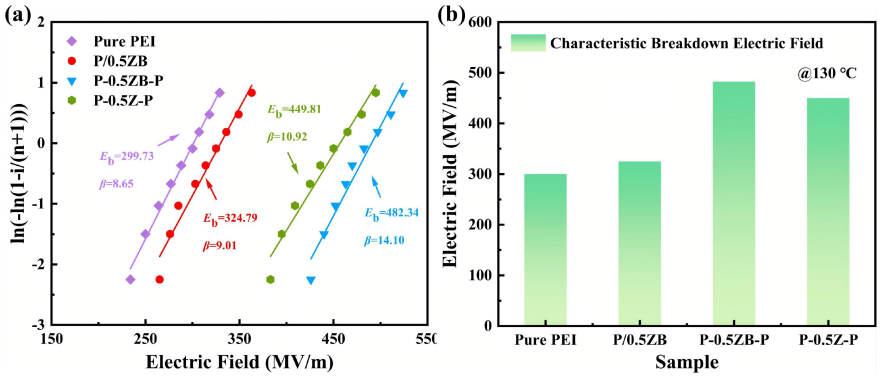

Fig. S17. (a) Weibull distribution and (b) characteristic breakdown strength of pure PEI, P/0.5ZB, P-0.5ZB-P, and P-0.5Z-P at 130 °C.

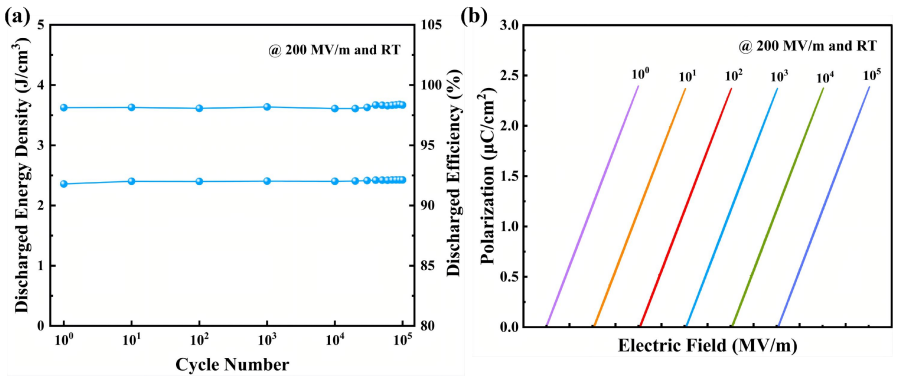

Fig. S18. Variation of U_e and η of the P-0.5ZB-P nanocomposite with cycle number under an applied electric field of 200 MV/m, with P- E cycles ranging from 1 to 10^5.

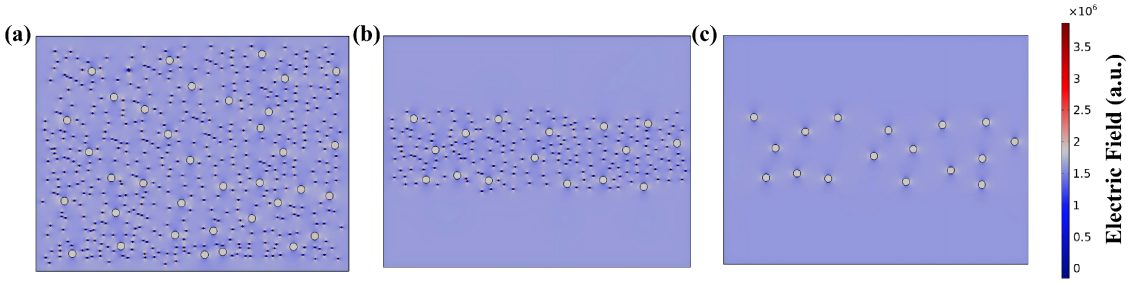

Fig. S19. The electric field distribution simulation images of (a) P/0.5Z, (b) P-0.5ZB-P, and (c) P-0.5Z-P.

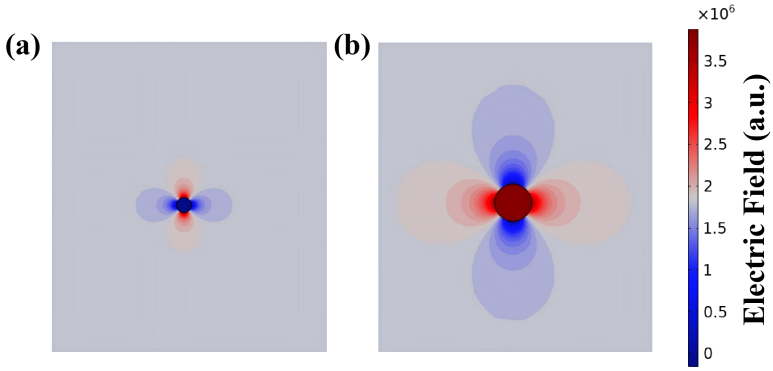

Fig. S20. Simulation results of electric field distribution for (a) $BaTiO_3$ NPs and (b) ZIF-67 in the PEI matrix.

1 V.P. Kallupadi, H. Varghese, U.N.S. Hareesh, A. Chandran. *Adv Funct Mater*, 2024, **35**, 2411855.

2 Y. Zidi, O. Khaldi, R.E. Patru, L.N. Leonat, M. Enculescu, V. Toma, A. Stepanova, R. Ben Younes, A.C. Galca. *Ceram Int*, 2025, **51**, 18166-18177.